Analysis of a Coextrusion Process for Preparing Gradient-Index Polymer Optical Fibers

ARTICLE *in* THE JOURNAL OF PHYSICAL CHEMISTRY B · SEPTEMBER 1999

Impact Factor: 3.3 · DOI: 10.1021/jp9911550

Theoretical Analysis on a Multilayer Coextrusion Process for Preparing Gradient-Index Polymer Optical Fibers

Wen-Chang Chen,* Yung Chang, and Jyh-Ping Hsu

Department of Chemical Engineering, National Taiwan University, Taipei, Taiwan 10617

Received: April 6, 1999; In Final Form: July 12, 1999

A theoretical analysis was conducted on a multilayer internal diffusion and surface evaporation (IDSE) coextrusion process for preparing gradient-index (GI) polymer optical fibers (POFs). The predicted refractive index distribution (RID) was in good agreement with the experimental data reported in the literature. The effects of the essential parameters, including the mass transfer coefficient of monomer across solid−gas interface, *k*, the diffusivities of monomers, and the radius ratio of each layer on RID were investigated. We show that if *k* is either very small or very large, then RID deviates significantly from a parabolic curve. The effect of the diffusivity of BzMA monomer on RID is more significant than that of MMA monomer. The results of numerical simulation reveal that both the radius ratio and the composition of each layer have significant effect on RID, and the greater the number of layers, the closer the RID is to a parabolic curve.

Introduction

Gradient-index (GI) polymer optical fibers (POFs) have attracted extensive interest in light of their versatile applications in optical communication, imaging, and collimating.[1−10] A GI POF based on perfluorinated (PF) polymer with an optical loss of 50 dB/km and a transmission speed of 2.5 Gb/s at 1.3 mm was prepared by Koike et al. recently.[3] It was reported that the theoretical attenuation limit of PF GI POF can be as low as 0.3 dB/km, which is comparable to that of a silica fiber in the near-infrared region. GI POF can also be used as an optical fiber amplifier by doping with organic dyes. Tagaya et al. demonstrated that after doping with organic dyes a GI POF becomes a high-gain, high energy conversion efficiency, and high-power optical amplifier.[11−13] Another potential usage of GI POF is that it can be used as the essential components of the selfoc lens array (SLA) used in fax machines and scanners.[14,15]

The refractive index distribution (RID) inside a GI POF can be described by

$$n(r) = n_1\left[1 - 2\delta\left(\frac{r}{R}\right)^g\right]^{1/2}, \quad 0 \le r \le R \tag{1}$$

$$\delta = \frac{n_1 - n_2}{n_1} \tag{2}$$

where n_1 and n_2 are respectively the refractive indices at the center axis and the periphery of an optical fiber, R is its radius, and g is a constant characterizing the RID. It was found that the bandwidth of a GI POF is maximized when g has the value of 2.[16] That is, the optimal RID is a parabolic curve.

The importance of GI POF stimulates several methods for preparing GI POFs. These include, for example, two-stage copolymerization,[17] photocopolymerization,[18] centrifugal molding,[19,20] interfacial gel copolymerization,[6,7,21,22] and a coextrusion process.[8,14,15,23] The differences between the monomer concentration, monomer reactivity, monomer size, monomer density, monomer diffusivity, the properties of the host polymers, and external process design are the basic design parameters for the production of an index gradient inside a fiber.

Multilayer coextrusion process is a versatile technology for preparing GI POF. The diffusion behavior of monomers through polymer mixture, and the mass transfer between the fiber periphery and the purged gas (for an open process) lead to an approximate quadratic RID. A two-layer closed coextrusion process was developed in our laboratory to produce GI POF.[8−10] The inner layer of the process was composed of poly(methyl methacrylate) (PMMA) and monomers benzyl methacrylate (BzMA) and methyl methacrylate (MMA), and the outer layer comprised PMMA and MMA. Mutual diffusion of BzMA and MMA occurred when the fiber precursor passed through the diffusion zone of the process. A theoretical analysis was conducted which is capable of predicting the RID inside a fiber.[24] It was found that RID depends largely upon several key parameters including the concentration and the diffusivities of monomers and the volume ratio of inner and outer layers. The result of numerical simulation revealed that only about 60% of a fiber prepared can have an approximate parabolic RID. This is mainly because the outer boundary of a closed coextrusion process is impermeable to BzMA, and therefore, the RID becomes flat near the peripheral region of a fiber. To improve its performance, an open, two-layer coextrusion process with internal diffusion and surface evaporation (IDSE) was developed recently to prepare GI POF.[15,25,26] This process has a purged nitrogen gas stream outside the periphery of a fiber precursor, and the outer boundary of the fiber precursor is permeable to monomers. Compared with a closed coextrusion process, an IDSE process was able to yield a larger portion of approximate parabolic RID.[25] However, it is almost impossible to obtain a complete parabolic RID in the radial direction of a fiber by varying the key parameters of the process. One of the possible ways to solve this problem is to increase the number of layers of an extrusion process. Toyoda et al.,[15] for example, developed a multilayer coextrusion process for preparing GI POF. They found that a parabolic RID could be achieved gradually by increasing the number of layers from three to five. The

* To whom correspondence should be addressed. Phone: 886-2-23628398. Fax: 886-2-23623040. E-mail: chenwc@ms.cc.ntu.edu.tw.

10.1021/jp9911550 CCC: $18.00
Published on Web 08/19/1999

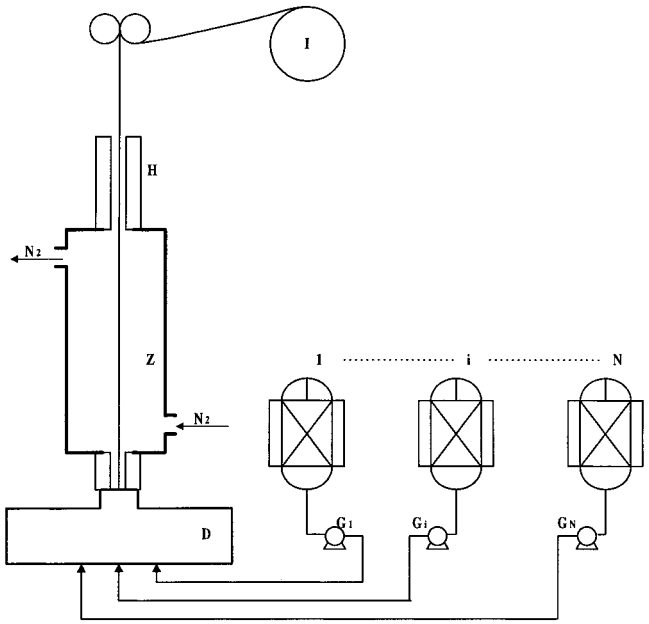

Figure 1. Schematic representation of a *N*-layer IDSE coextrusion process. G_1, G_2, ..., G_N represent gear pumps, D is concentric die, Z and H are the diffusion zone and hardening zone, respectively, and I is take-up roll.

conclusion of Toyoda et al.[15] is of practical significance. However, since their observation was based on an experimental study, the effect of the key parameters of a process on its performance needs to be conducted on a trial-and-error type of approach. This is undesirable from the process design and control point of view, and a study based on theoretical analysis is necessary.

In the present study, a general *N*-layer IDSE coextrusion process is modeled. An analytical expression is derived, and its applicability is examined by fitting the experimental data of Toyoda et al.[15] The performance of a process is also investigated by varying its key parameters, which include the number of layers, radius ratio of each layer, the mass transfer coefficient of diffusion reagent, and the diffusivities of monomers.

Modeling

Referring to Figure 1, we consider an *N*-layer IDSE coextrusion process for preparing GI POF. Material tanks 1, 2, ..., *N* containing the solution of a polymer and monomers were heated at a sufficiently high temperature. The contents of each tank was fed by the gear pumps G_1, G_2, ..., G_N to a concentric die D. The tanks are arranged so that the RIs of the contents inside the concentric die were in a decreasing order from the center to the periphery of the die. The volume ratios of the polymer solutions from different tanks can be adjusted so that RID can be varied. An *N*-layer composite monofilament was then extruded out of the orifice of the die and fed into a diffusion zone Z with length *L*. While the monofilament went through the diffusion zone, the monomers contained in each layer diffused across the monofilament leading to a certain RID. A hot nitrogen gas was purged through the diffusion zone, and mass transfer between the gas phase and monofilament was allowed to occur, which will also affect the RID of the latter. The monofilament was then fed through a hardening zone H where it was hardened by UV lamps. A polymer fiber with a certain RID was taken up through rolls by a take-up roll, I.

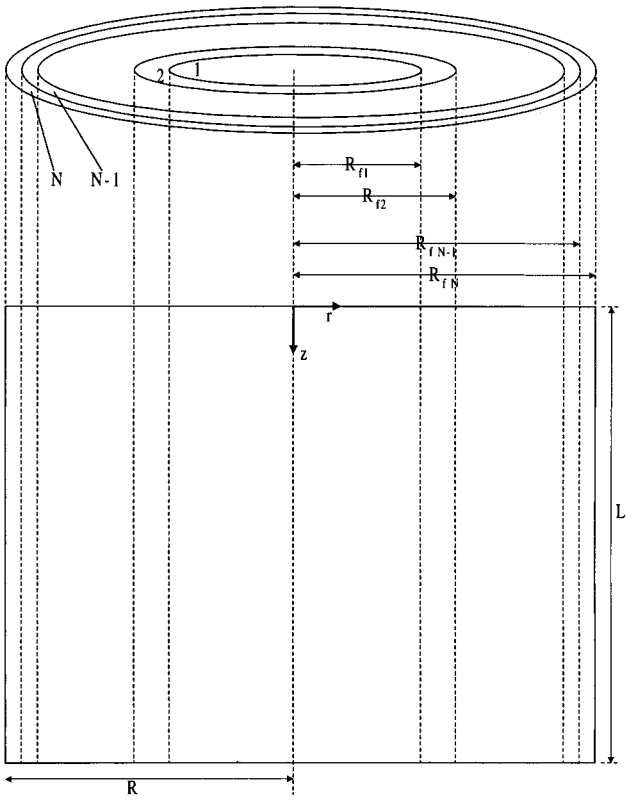

Figure 2. Coordinates adopted in the mathematical modeling. *r* and *z* are the radial and axial distances, respectively, *L* is the length of diffusion zone, R_{f1}, R_{f2}, ..., R_{fN} are the radius of each layer.

Figure 2 shows the coordinates adopted in the mathematical modeling. Here, R_{fi} denotes the radius of *i*th layer and *R* is the radius of the diffusion zone. Let *r* and *z* be the radial distance and the distance from the entrance of the diffusion zone, respectively. Suppose that the process is operated under an isothermal condition and the diffusivities of monomers are functions of the mass fraction of host polymer only. Since the density of the filament remains approximately the same in the diffusion zone, we assume that the change in the bulk density of the filament is negligible. Suppose that the diffusion of monomers during the hardening period is negligible. In this case, the variation of the mass fraction of monomer M, *x*, at a steady-state operation can be described by

$$u\frac{\partial x}{\partial z} = D_r\left(\frac{\partial^2 x}{\partial r^2} + \frac{1}{r}\frac{\partial x}{\partial r}\right) + D_z\frac{\partial^2 x}{\partial z^2} \tag{3}$$

where *u* denotes the extrusion velocity, and D_r and D_z are the effective diffusivities of monomers in the *r* and *z* directions, respectively. The boundary conditions associated with eq 3 are summed as

$$x \text{ is finite at } r = 0 \tag{4a}$$

$$-D_r\frac{\partial x}{\partial r} = kx \text{ at } r = R \tag{4b}$$

Here, *k* represents the mass transfer coefficient of monomer M between the fiber periphery and the gas phase. Under conditions of practical significance, the Peclect number (uL/Dz) is large; that is, the transport of the monomers due to convection motion dominates that due to molecular diffusion. Therefore, the last term on the right-hand side of eq 3 is much smaller than the term on the left-hand side and can be neglected. In this case,

eq 3 can be rewritten in the following dimensionless form:

$$\frac{\partial x^*}{\partial z^*} = \frac{\partial^2 x^*}{\partial r^{*2}} + \frac{1}{r^*}\frac{\partial x^*}{\partial r^*} \tag{5}$$

where $x^* = x/x_0$, $r^* = r/R$, and

$$z^* = \frac{zD_r}{uR^2} \tag{5a}$$

$$k^* = \frac{kR}{D_r} \tag{5b}$$

In these expressions, x_0 represents the mass fraction of monomer M at $z = 0$. The corresponding boundary conditions become

$$x^* \text{ is finite at } r^* = 0 \tag{6a}$$

$$\frac{\partial x^*}{\partial r^*} = -k^* x^* \text{ at } r^* = 1 \tag{6b}$$

Three kinds of monomers with different refractive indices, MMA, BzMA, and FPMA, were used in this study. The dimensionless mass fraction x can be defined as

$$x^*_{\mathrm{M}} = x_{\mathrm{M},i}/x_{\mathrm{M,L}},\ i = 1, 2, ..., N \tag{7a}$$

where $x_{\mathrm{M},i}$ and $x_{\mathrm{M,L}}$ are the mass fraction of monomer M in the ith layer and the highest concentration of monomer M in the ith layer at $z = 0$, respectively. Equation 5b can rewritten, for each monomer, as

$$z^*_{\mathrm{BzMA}} = \frac{zD_{\mathrm{BzMA}}}{uR^2} \tag{7b}$$

$$z^*_{\mathrm{MMA}} = \frac{zD_{\mathrm{MMA}}}{uR^2} \tag{7c}$$

$$z^*_{\mathrm{FPMA}} = \frac{zD_{\mathrm{FPMA}}}{uR^2} \tag{7d}$$

The dimensionless radius of each layer can be expressed by

$$R^*_{\mathrm{f}i} = R_{\mathrm{f}i}/R, \quad i = 1, 2, ..., N \tag{7e}$$

where $R^*_0 = 0$ and $R^*_{fN} = 1$. Solving eq 5 subject to eqs 6a−7e gives the variation of the concentration of monomers M,

$$x^*_{\mathrm{M}} = 2\sum_{m=1}^{\infty} \left(\frac{k^* x^*_{\mathrm{M},N} J_0(\lambda_m) + \sum_{i=2}^{N} (x^*_{\mathrm{M},i-1} - x^*_{\mathrm{M},i}) \lambda_m R^*_{\mathrm{f}_{i-1}} J_1(\lambda_m R^*_{\mathrm{f}_{i-1}})}{J_0^2(\lambda_m)(k^{*2} + \lambda_m^2)} \right) \times \exp(-\lambda_m^2 z^*_{\mathrm{M}}) J_0(\lambda_m r^*) \tag{8}$$

The dimensionless mass fractions of BzMA, MMA, and FPMA monomers at the outlet of the diffusion zone ($z = L$), x^*_{BzMA}, x^*_{MMA}, and x^*_{FPMA} respectively, can be obtained from this expression as

$$x^*_{\mathrm{BzMA}} = 2\sum_{m=1}^{\infty} \left(\frac{k^* x^*_{\mathrm{BzMA},N} J_0(\lambda_m) + \sum_{i=2}^{N} (x^*_{\mathrm{BzMA},i-1} - x^*_{\mathrm{BzMA},i}) \lambda_m R^*_{\mathrm{f}_{i-1}} J_1(\lambda_m R^*_{\mathrm{f}_{i-1}})}{J_0^2(\lambda_m)(k^{*2} + \lambda_m^2)} \right) \times \exp(-\lambda_m^2 z^*_{\mathrm{BzMA}}) J_0(\lambda_m r^*) \tag{9}$$

$$x^*_{\mathrm{MMA}} = 2\sum_{m=1}^{\infty} \left(\frac{k^* x^*_{\mathrm{MMA},N} J_0(\lambda_m) + \sum_{i=2}^{N} (x^*_{\mathrm{MMA},i-1} - x^*_{\mathrm{MMA},i}) \lambda_m R^*_{\mathrm{f}_{i-1}} J_1(\lambda_m R^*_{\mathrm{f}_{i-1}})}{J_0^2(\lambda_m)(k^{*2} + \lambda_m^2)} \right) \times \exp(-\lambda_m^2 z^*_{\mathrm{MMA}}) J_0(\lambda_m r^*) \tag{10}$$

$$x^*_{\mathrm{FPMA}} = 2\sum_{m=1}^{\infty} \left(\frac{k^* x^*_{\mathrm{FPMA},N} J_0(\lambda_m) + \sum_{i=2}^{N} (x^*_{\mathrm{FPMA},i-1} - x^*_{\mathrm{FPMA},i}) \lambda_m R^*_{\mathrm{f}_{i-1}} J_1(\lambda_m R^*_{\mathrm{f}_{i-1}})}{J_0^2(\lambda_m)(k^{*2} + \lambda_m^2)} \right) \times \exp(-\lambda_m^2 z^*_{\mathrm{FPMA}}) J_0(\lambda_m r^*) \tag{11}$$

In these expressions J_0 and J_1 are the Bessel functions of the first kind of orders 0 and 1, respectively, and λ_m is the positive root of $k^* J_0(\lambda_m) = \lambda_m J_1(\lambda_m)$.

Asymptotic Cases

Two asymptotic cases can be recovered directly from the present model: $k^* \to 0$ and $k^* \to \infty$. The former is equivalent to a closed coextrusion process. If $k^* \to 0$, eq 8 reduces to

$$x^*_{\mathrm{M}} = x^*_{\mathrm{M},N} + \sum_{i=2}^{N} (x^*_{\mathrm{M},i-1} - x^*_{\mathrm{M},i}) R^{*2}_{\mathrm{f}_{i-1}} + 2\sum_{m=1}^{\infty} \frac{\sum_{i=2}^{N} (x^*_{\mathrm{M},i-1} - x^*_{\mathrm{M},i}) R^*_{\mathrm{f}_{i-1}} J_1(\lambda_m R^*_{\mathrm{f}_{i-1}})}{\beta_m J_0^2(\beta_m)} \times \exp(-\lambda_m^2 z^*_{\mathrm{M}}) J_0(\lambda_m r^*) \tag{12}$$

where λ_m is the root of $J_1(\lambda_m) = 0$. The other extreme, $k^* \to \infty$, implies that a perfect permeability at the outer boundary of the diffusion zone. In this case, eq 8 becomes

$$x^*_{\mathrm{M}} = 2\sum_{m=1}^{\infty} \left(\frac{x^*_{\mathrm{M},N} \lambda_m J_1(\lambda_m) + \sum_{i=2}^{N} (x^*_{\mathrm{M},i-1} - x^*_{\mathrm{M},i}) \lambda_m \mathrm{R}^*_{\mathrm{f}_{i-1}} J_1(\lambda_m \mathrm{R}^*_{\mathrm{f}_{i-1}})}{\lambda_m^2 J_1^2(\lambda_m)} \right) \times \exp(-\lambda_m^2 z^*_{\mathrm{M}}) J_0(\lambda_m r^*) \tag{13}$$

where λ_m is the positive root of $J_0(\lambda_m) = 0$.

The transformation of the fiber composition to RID can be performed as below. Lorentz and Lorenz[27,28] suggested that the optical property of a nonabsorbing media and its chemical structure correlate through an additive rule. The RI of a composite material, for example, can be represented by[29]

$$n_d = \sqrt{\frac{1+2\phi}{1-\phi}} \tag{14}$$

with

$$\phi = \frac{\sum_M \frac{{n_{d,M}}^2 - 1}{{n_{d,M}}^2 + 2} \frac{x_M}{\rho_M}}{\sum_M \frac{x_M}{\rho_M}} \tag{14a}$$

where $n_{d,M}$ and ρ_M are the RI and density of the component M. Therefore, the RI of a GI POF produced by the *N*-layer extrusion process can be determined by the combination of eqs 9−11 and 14. The index exponent *g* of the RID can be estimated by fitting the predicted data with eq 1. Define $\Delta n = n_1 - n_2$, with n_1 and n_2 being the RI at the center and periphery of a fiber.

Results and Discussion

The applicability of the present model is justified by fitting it to the experimental data of Toyoda.[15] Their experimental conditions are summarized in Table 1.

Three-Layer IDSE Process. Figure 3 shows the variation of the RI of a GI POF, *n*, as a function of its dimensionless radius *r**. Both the results predicted by the present model and the experimental data of Toyoda[15] are presented. In the data fitting procedure, since the effective diffusivities of MMA and BZMA monomers were not available at hand, they were treated as adjustable parameters. The estimated values of D_{BZMA} and D_{MMA}, based on a least-squares criterion, are both 9×10^{-6} cm^2/s, which has the same order of magnitude as the diffusivity of a small molecule in PMMA.[22] Note that MMA and BzMA monomers might interfere with each other, and therefore, their diffusion coefficients might be indistinguishable.[30] The estimated value for the mass transfer coefficient *k* is 7.5×10^{-4} cm/s, which is in the reasonable range.[31] The estimated values of Δn and g are 0.012 and 2.198, respectively. As can be seen from Figure 3, the performance of the present model is satisfactory.

Effects of Key Parameters on RID for Three-Layer IDSE Process. Figure 4 shows the simulated RID of a fiber at various k^* for a three-layer IDSE co-extrusion process. The values of Δn and *g* for $k^* = 0$ (curve a) are 0.00188 and 1.014, respectively. According to eq 5b, $k^* = 0$ implies that $k = 0$ or $D_r \rightarrow \infty$. The former is equivalent to a closed coextrusion process, and the latter implies that the distributions of monomers are uniform, which leads to a almost flat RID. For the case of curve b, $k^* = 5$, the estimated Δn and *g* are 0.012 and 2.198, respectively, and the RID is close to a parabolic curve. If $k^* \rightarrow \infty$ (curve c), the estimated Δn and *g* are 0.0329 and 1.554, respectively. $k^* \rightarrow \infty$ implies a very large mass transfer coefficient *k* or a very small diffusion coefficient D_r. Note that the only monomer present in the outmost layer is MMA, which a relatively low RI. A large *k* implies that a large amount of MMA will be driven out of the fiber to the gas phase. On the other hand, it is relatively difficult for BzMA monomer, which has a high RI, in the central part of a fiber to be driven out of the fiber. This is why the Δn for the case of curve c is larger than that for the case of curve b. If D_r is small, most of BzMA monomers are kept in the central portion and MMA monomers in the outer layer. This also yields a large Δn. However, the value of *g* decreases also, and the corresponding RID deviates from a parabolic curve. This is because that Δn is too large. The above discussions suggest that there exists an optimum *k*.

Figure 5 shows the simulated RID at various Z^*_{MMA}. As can be seen from this figure, the conditions lead to curve a is

TABLE 1: Experimental Conditions Used by Toyoda et al.[15] [a]

item	three-layer	four-layer	five-layer
	Mixture 1 (inner layer)		
PMMA (%)	52	52	52
BzMA (%)	35	35	35
MMA (%)	13	13	13
	Mixture 2 (second layer)		
PMMA (%)	50	50	50
BzMA (%)	15	15	15
MMA (%)	35	35	35
	Mixture 3 (third layer)		
PMMA (%)	50	50	50
BzMA (%)			
MMA (%)	50	50	50
	Mixture 4 (fourth layer)		
PMMA (%)		47	47
BzMA (%)			
MMA (%)		40	40
FPMA (%)		13	13
	Mixture 5 (outer layer)		
PMMA (%)			40
BzMA (%)			
MMA (%)			18
FPMA(%)			42
R (mm)	0.59	0.6	0.6
radius ratio (3-layer)	$0.76(R^*_{f1}):0.96(R^*_{f2}):1(R^*_{f3})$		
radius ratio (4-layer)	$0.75(R^*_{f1}):0.94(R^*_{f2}):0.98(R^*_{f3}):1(R^*_{f4})$		
radius ratio (5-layer)	$0.73(R^*_{f1}):0.92(R^*_{f2}):0.96(R^*_{f3}):0.98(R^*_{f4}):1(R^*_{f5})$		
T (°C)	60		
u (cm/min)	40		
L (cm)	45		

[a] The RI values of PMMA, Poly(BzMA), and Poly(FPMA) used in the present study are 1.491, 1.568, 1.49, and 1.395, respectively. The densities of PMMA, BzMA, MMA, and FPMA used in the present study are 1.141, 0.935, 0.896, and 1.356 g/cm^3, respectively.

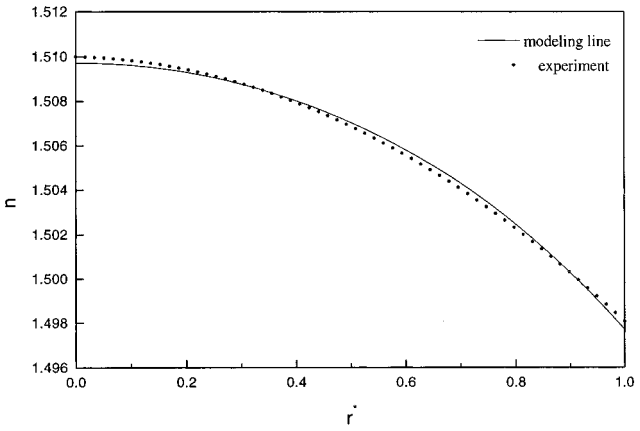

Figure 3. Variation of RI of a fiber *n* as a function of its dimensionless radius, *r**. The experimental conditions are shown in column 1 of Table 1. The estimated values of the adjustable parameters are $k^* = 5$, $Z_{BzMA}^* = 0.17$, $Z_{MMA}^* = 0.17$. Dashed line, experimental data; solid line, values based on the present model.

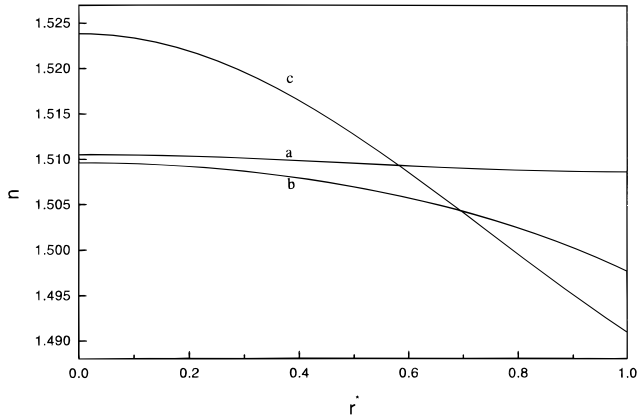

Figure 4. Simulated RID of a fiber at various k^*. Curve a, $k^* \rightarrow 0$; curve b, $k^* = 5$; curve c, $k^* \rightarrow \infty$. The experimental conditions are shown in column 1 of Table 1. Parameters used are $Z_{BzMA}^* = 0.17$, $Z_{MMA}^* = 0.17$, $R_{f1}^* = 0.76$, and $R_{f2}^* = 0.96$.

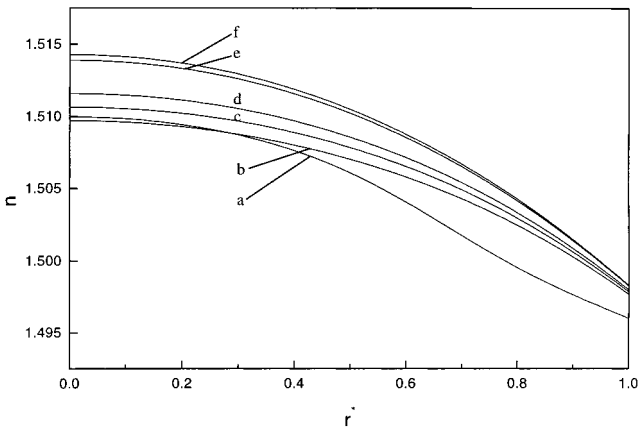

Figure 5. Simulated RID of a fiber at various Z_{MMA}^*. Curve a, $Z_{MMA}^* = 0.017$; curve b, $Z_{MMA}^* = 0.17$; curve c, $Z_{MMA}^* = 0.25$; curve d, $Z_{MMA}^* = 0.34$; curve e, $Z_{MMA}^* = 0.85$; curve f, $Z_{MMA}^* = 1.7$. The experimental conditions are shown in column 1 of Table 1. Parameters used are $Z_{BzMA}^* = 0.17$, $R_{f1}^* = 0.76$, and $R_{f2}^* = 0.96$.

inadequate since the deviation from a parabolic curve is significant. As Z^*_{MMA} increases from 0.017 (curve b) to 1.7 (curve f), g decreases from 2.198 to 2.083, and Δn increases from 0.012 to 0.160. That is, the larger the Z^*_{MMA} the closer an RID is to a parabolic curve. According to eq 7c, if all the other parameters are fixed, a large Z^*_{MMA} implies a large diffusion coefficient D_{MMA}. As D_{MMA} increases, the rate of diffusion of MMA monomer, which has a low RI, increases accordingly, which results in a decreasing ratio of MMA monomer in each layer of a fiber. Since the rate of diffusion of BzMA monomer is fixed, Δn increases, as can be seen from Figure 5.

Figure 6 illustrates the simulated RID at various Z^*_{BZMA}. The estimated values of g for curves a−f are 4.016, 2.198, 2.105, 2.039, 1.869, and 2.340, respectively, and the corresponding values of Δn are 0.0145, 0.0120, 0.0098, 0.0075, 0.0011, and −0.0001, respectively. As Z^*_{BZMA} increases from 0.017 (curve a) to 0.17 (curve f), the value of g first decreases from 4.016 (curve a) to 1.869 (curve e) and then increases to 2.340 (curve f). This behavior can be elaborated as below. According to eq 7b, if all the other parameters are fixed, a small Z^*_{BzMA} implies a small D_{BzMA}, and the diffusion of BzMA monomer is slow. In this case, BzMA monomer tends to stay near the center portion of a fiber, which leads to a flat RID near there, and a rapid drop near its peripheral portion, as shown in curve a of Figure 6. As Z^*_{BzMA} increases, more BzMA monomers are

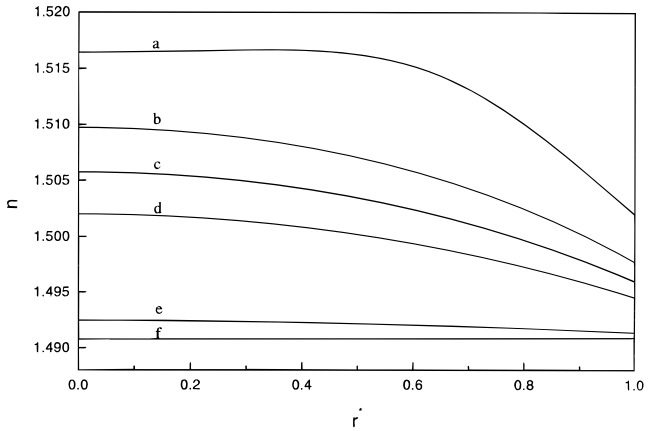

Figure 6. Simulated RID of a fiber at various Z_{BZMA}^*. Curve a, $Z_{BZMA}^* = 0.017$; curve b, $Z_{BZMA}^* = 0.17$; curve c, $Z_{BZMA}^* = 0.25$; curve d, $Z_{BZMA}^* = 0.34$; curve e, $Z_{BZMA}^* = 0.85$; curve f, $Z_{BZMA}^* = 1.7$. The experimental conditions are shown in column 1 of Table 1. Parameters used are $Z_{MMA}^* = 0.17$, $R_{f1}^* = 0.76$, and $R_{f2}^* = 0.96$.

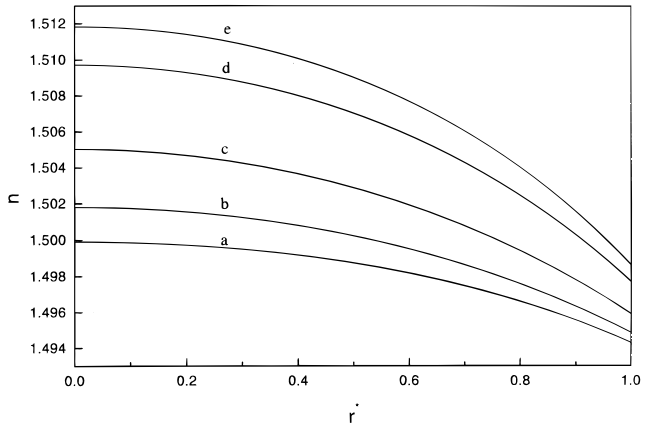

Figure 7. Simulated RID of a fiber at various R_{f1}^*. Curve a, $R_{f1}^* = 0.1$; curve b, $R_{f1}^* = 0.3$; curve c, $R_{f1}^* = 0.5$; curve d, $R_{f1}^* = 0.76$; curve e, $R_{f1}^* = 0.9$. The experimental conditions are shown in column 1 of Table 1 except R_{f1}^*. Parameters used are $Z_{MMA}^* = 0.17$, $Z_{BzMA}^* = 0.17$, and $R_{f2}^* = 0.96$.

capable of diffusing into the periphery portion of a fiber, and the value of g gradually approaches that of a parabolic curve. However, if Z^*_{BzMA} is too large, most of BzMA monomers diffuse out the center portion of the fiber, which leads to a small Δn and a small g. A comparison between Figures 5 and 6 reveals that Z^*_{BzMA} has a more significant effect of on the RID of a fiber than Z^*_{MMA}. In other words, BzMA plays a more significant role than MMA for the process under consideration.

Figure 7 shows the simulated RID at various R^*_{f1}. As R^*_{f1} varies from 0.1 (curve a) to 0.9 (curve e), Δn increases from 0.006 to 0.013. As illustrated in Table 1, the first layer contains 35% BzMA monomer. Therefore, an increase in R^*_{f1} is equivalent to increase the amount of high RI component, which leads to a large Δn. However, if R^*_{f1} is too large, the rate of decrease in RID as the peripheral zone of a fiber is approached may become too fast. This is reflected by the variation of g for the RID presented in Figure 7. Here, g first decreases from 2.309 (curve a) to 2.113 (curve c) and then increases again to 2.280 (curve e). This suggests that there exist an optimum R^*_{f1}.

Figure 8 illustrates the simulated RID at various R^*_{f2}. As R^*_{f2} varies from 0.8 to 0.98 Δn increases from 0.0112 (curve a) to 0.0121 (curve e). That is, although Δn increases with R^*_{f2}, the rate of increase is less significant that that for the case of R^*_{f1}. This is mainly because that the range of the volume

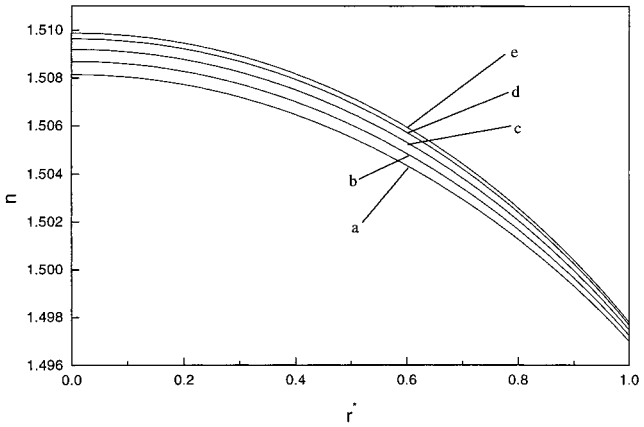

Figure 8. Simulated RID of a fiber at various R_{f2}*. Curve a: R_{f2}* = 0.8; curve b, R_{f2}* = 0.85; curve c, R_{f2}* = 0.90; curve d, R_{f2}* = 0.95; curve e, R_{f2}* = 0.98. The experimental conditions are shown in column 1 of Table 1 except R_{f1}*. Parameters used are Z_{MMA}* = 0.17, Z_{BzMA}* = 0.17, and R_{f1}* = 0.76.

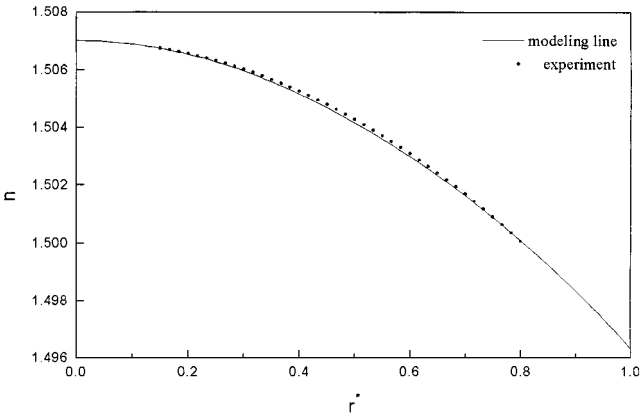

Figure 9. Variation of RI of a fiber *n* as a function of its dimensionless radius, *r**. The experimental conditions are shown in column 2 of Table 1. The estimated values of the adjustable parameters are *k** = 5, Z_{BzMA}* = 0.1, Z_{MMA}* = 0.2, Z_{FPMA}* = 0.165. Dashed line, experimental data; solid line, value based on the present model.

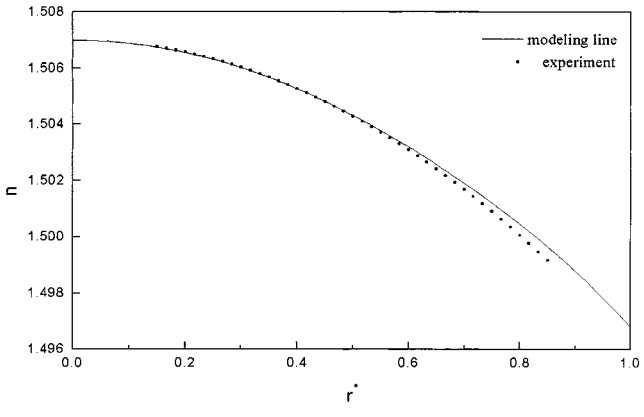

Figure 10. Variation of RI of a fiber *n* as a function of its dimensionless radius, *r**. The experimental conditions are shown in column 3 of Table 1. The estimated values of the adjustable parameters are *k** = 5, Z_{BzMA}* = 0.075, Z_{MMA}* = 0.075, Z_{FPMA}* = 0.545. Dashed line, experimental data; solid line, values based on the present model.

ratio examined is limited and the high RI BzMA monomer is only 15% in the second layer (Table 1).

Four- and Five-Layer IDSE Processes. Figures 9 and 10 show the RID for four- and a five-layer IDSE coextrusion processes, respectively. Both the results predicted by the present model and the experimental data of Toyoda[15] are illustrated. As can be seen from these figures, the performance of the present model is satisfactory for both processes. The estimated values of *g* for the four- and the five-layer IDSE processes are 1.925 and 1.953, respectively. Since the estimated value of *g* based on the results shown in Figure 3 for the case of a three-layer IDSE process is 2.198, we conclude that the more the number of layers, the closer the RID to a parabolic curve.

Conclusions

A theoretical modeling was successfully developed to predict the multilayer IDSE coextrusion process for preparing GI POFs. Optimum essential parameters were required for the parabolic RID in the studied three-layer system. Although the Δn value was enhanced as *k** approached infinite, it decrease to a small value as *k** close to zero. As *k** came close to a very small value or a very large value, the RID deviated significantly from the parabolic RID. The diffusion rate of the monomer BzMA showed a more significant effect on the RID than that of MMA since BzMA controlled the RI difference in each layer. The radius ratio and the composition of each layer are both required to be considered for obtaining the parabolic RID. The greater the number of layers of a coextrusion process, the closer the RID is to a parabolic curve.

Acknowledgment. This work was supported by the National Science Council of the Republic of China under Grant No. NSC 87-2216-E002-019.

References and Notes

(1) Bourdinaud, M., Ed. *Proceeding of 5th International Conference on Plastic Optical Fibers and Applications*; Paris, France, October 22−24, 1996.
(2) Talukder, M., Koike, Y., Eds. *Proceeding of POF Conference '97*; Kauai, Hawaii, September 22−25, 1997.
(3) Koike, Y., Ed. *Proceeding of 7th International Conference on Plastic Optical Fibers and Applications*; Berlin, October 5−8, 1998.
(4) Kaino, T. *Polymers for Lightwave and Integrated Optics*; Hornak, L. A., Ed.; Marcel Dekker: New York, 1992; Chapter 1.
(5) Koike, Y. *Polymer* **1991**, *32*, 1737.
(6) Yang, S. Y.; Chang, Y. H.; Ho, B. C.; Chen, W. C.; Tseng, T. W. *Polym. Bull.* **1995**, *34*, 87.
(7) Yang, S. Y.; Chang, Y. H.; Ho, B. C.; Chen, W. C.; Tseng, T. W. *J. Appl. Polym. Sci.* **1995**, *56*, 1179.
(8) Ho, B. C.; Chen, J. H.; Chen, W. C.; Yang, S. Y.; Chen, J. J.; Tseng, T. W. *Polymer J.* **1995**, *27*, 310.
(9) Chen, W. C. Chen, J. H.; Yang, S. Y.; Cherng, J. Y.; Chang, Y. H.; Ho, B. C. *J. Appl. Polym. Sci.* **1996**, *60*, 1379.
(10) Chen, W. C.; Chen, J. H.; Yang, S. Y.; Chen, J. J.; Chang, Y. H.; Ho, B. C.; Tseng, T. W. *ACS Symp. Ser.* **1997**, *672*, 71.
(11) Tayaga, A.; Koike, Y.; Nihei, E.; Teramoto, S.; Fujii, K.; Yamamoto, T.; Sasaki, K. *Appl. Opt.* **1995**, *34*, 8.
(12) Tagaya, A.; Kobayashi, T.; Nakatsuka, S.; Nihei, E.; Sasaki, K.; Koike, Y. *Jpn. J. Appl. Phys.* **1997**, *36*, 2705.
(13) Tagaya, A.; Teramoto, S.; Nihei, E.; Sasaki, K.; Koike, Y. *Appl. Opt.* **1997**, 572.
(14) Yamamoto, T.; Mishina, Y.; Oda, M. U.S. Patent 4,582,982, August, 1989.
(15) Toyoda, N.; Mishina, Y.; Murata, R.; Uozu, Y.; Oda, M.; Ishimaru, T. U.S. Patent 5,390,274, February, 1995.
(16) Olshansky, R.; Keck, D. B. *Appl. Opt.* **1976**, *15*, 483.
(17) Ohtsuka, Y. *Appl. Phys. Lett.* **1973**, *23*, 2347.
(18) Ohtsuka, Y.; Nakamoto, I. *Appl. Phys. Lett.* **1976**, *29*, 559.
(19) Hamblen, D. P. U.S. Patent 4,022,855, May, 1977.
(20) Duijhoven, F. G. H.; Bastiaansen, C. W. M. In Koike, Y., Ed. *Proceeding of 7th International Conference on Plastic Optical Fibers and Applications*; Berlin, October 5−8, 1998; 55.
(21) Koike, Y.; Takezawa, Y.; Ohtsuka, Y. *Appl. Opt.* **1990**, *29*, 2686.
(22) Zhang, Q.; Wang, P.; Zhai, Y. *Macromolecules* **1997**, *30*, 7874.
(23) Perry, G. A.; Witcher, C. E. U.S. Patent 5,235,660, August, 1993.
(24) Liu, B.-T.; Chen, W. C.; Hsu, J.-P. *Polymer* **1999**, *40*, 1451−1457.
(25) Liu, B.-T.; Hsieh, M.-Y.; Chen, W. C.; Hsu, J.-P. *Polymer J.* **1999**, *31*, 233.
(26) Tsai, C. C.; Liu, T. J.; Chang, Y. H.; Tseng, T. W. *Chem. Eng. Sci.* **1997**, *52*, 221.

(27) Lorentz, H. A. *Wied. Ann. Phys.* **1880**, *9*, 641.
(28) Lorenz, L. V. *Wied. Ann. Phys.* **1880**, *11*, 70.
(29) Van Krevelen, D. W. *Properties of Polymers*, 3rd ed.; Elsevier: Amsterdam, The Netherlands, 1990; Chapter 10.
(30) Von Meerwall, E. An internal report to Industrial Technology Research Institute, Hsinchu, Taiwan, 1994.
(31) Trebal, R. E. *Mass Transfer Operations*; McGraw-Hill: New York, 1980.